# In-situ grown of FeCo<sub>2</sub>O<sub>4</sub> onto 2D-Carbyne coated nickel foam - A newer nanohybrid electrode for high performance supercapacitor

Preethi Dhandapani<sup>a</sup>, BalakrishnanBalan<sup>a</sup>, Tandabany Dinadayalane<sup>b</sup>, Subramania Angaiah<sup>a\*</sup>

<sup>a</sup>Electro-Materials Research Laboratory, Centre for Nanoscience and Technology,
Pondicherry University, Puducherry, 605014, India

<sup>b</sup>Department of Chemistry, Clark Atlanta University, Atlanta, GA 30314, USA

\*Corresponding Author, E-mail: a.subramania@gmail.com

# **Abstract**

In this study, we synthesized carbyne by a simple chemical route and then this was coated on nickel foam. On this carbyne coated nickel foam,  $FeCo_2O_4$  was grown by the solvothermal process to serve as a nanohybrid electrode for supercapacitor applications. This nanohybrid electrode has shown high specific capacitance due to the large surface area, high electrical conductivity and improved rate characteristics. The specific capacitance of  $FeCo_2O_4$  @ Carbyne nanohybrid electrode was about 2584.8  $Fg^{-1}$  at the current density of 3  $Ag^{-1}$ . Furthermore, the asymmetric supercapacitor device integrated with  $FeCo_2O_4$  @ Carbyne and activated carbon ( $FeCo_2O_4$  @ Carbyne || AC) shows better performance with an energy density of about 96.59 Wh  $Kg^{-1}$  at a high-power density of 2.25 kW  $kg^{-1}$  with a capacitance decay of about 14.52 % even at 5000 cycles. These outcomes provide a new approach for the development of supercapacitors with superior characteristics.

# **KEYWORDS**

FeCo<sub>2</sub>O<sub>4</sub>, Carbyne, Nanohybrid electrode, Solvothermal process, Supercapacitor, Specific capacitance.

#### INTRODUCTION

Due to continuous increase in global population, energy crises have become one of the most crucial problems and it is mainly due to the over usage of conventional resources[1]. Confronted with a serious problem of energy crises and environmental pollution, the desire for fabricating green and renewable energy sources is becoming significantly important[2,3]. In such a case, energy harvesting and energy storage are used as technology. Among the devices developed for better energy harvesting and energy storage, battery and supercapacitor have been used extensively[4,5]. In general, batteries are energy storage devices in which reversible electrochemical reaction allows the storage of electrical energy as Columbic potential and releases the energy on demand, but with a limited life cycle[6]. The efforts toward increasing the life cycle of batteries led to the invention of supercapacitors[7],[8]. Of various known energy storage devices, the supercapacitor works and stores energy either based on the electrochemical double layer or pseudocapacitor effect[9]. The electrode materials for electrochemical double layer capacitor (EDLC) are carbon-based materials such as graphite, carbon nanotubes (CNTs), and graphene, which has large surface area and normally form a double layer at the electrode/electrolyte interface[10],[11]. On the other hand, pseudocapacitance which arises from the reversible faradaic redox process provides enhanced electrocapacitive performance compared to EDLC's effect. The used electrodes can be of conducting polymers, metal oxides, hydroxides, and transition metal oxides[12]. However, the decreased rate capability is due to lower electron transport that limits the usage of transition metal oxides[13]. This can be overcome by making use of mixed transition metal oxides ( $MCo_2O_4$ , where M = Ni, Fe, Sn, Mn, Cu).

Owing to their multiple oxidation states, mixed transition metal oxide electrodes are attracted current interest for the enhanced electrochemical performance than the electrodes of individual transition metal oxides[14]·[15]. Of various mixed transition metal oxides, FeCo<sub>2</sub>O<sub>4</sub> has much valuable positivity such as low cost, environmentally friendly, less toxicity, wide availability, better electronic conductivity and higher capacitance, which have fascinated much attention. Besides the mechanism, the surface phenomena hold a significant place. The surface phenomena of the material such as a larger surface area and suitable porous structure lead to the higher capacitance which facilitates electron transport and shortens the transmission distance. Hence, the researchers are focusing on developing the electrode material on the three-dimensional conducting surface such as Ni foam[16]. Recently, NF@NCO/NCO NFA

nanocomposite prepared by Kumar et al. exhibits a specific capacitance of about 2314 Fg<sup>-1</sup> corresponding to 2 mAcm<sup>-2</sup> with excellent cyclic stability[17]. Further, Zhang et al. fabricated mesoporous spinel NiCo<sub>2</sub>O<sub>4</sub> via a hydrothermal process that exhibits a specific capacitance of about 1619.1 Fg<sup>-1</sup> at 2 Ag<sup>-1</sup>[18]. Meanwhile, Yua et al. fabricated NiCo<sub>2</sub>O<sub>4</sub> on nickel foam which results in a better performance of about 1450 Fg<sup>-1</sup> at 20 Ag<sup>-1</sup> [19]. Though various mixed transition metal oxides are available, the usage of FeCo<sub>2</sub>O<sub>4</sub> as electrode had been rarely reported. For example, Nilesh et al. fabricated FeCo<sub>2</sub>O<sub>4</sub> nanowires which exhibit specific capacitance of 1963 Fg<sup>-1</sup> in neutral electrolyte[20]. Similarly, Saad et al. fabricated FeCo<sub>2</sub>O<sub>4</sub> nanoflakes which exhibits specific capacitance of 433 Fg<sup>-1</sup> at 0.1 Ag<sup>-1</sup> in non-aqueous electrolyte. However, the specific capacitance exhibited by FeCo<sub>2</sub>O<sub>4</sub> electrode is low because of lower ion diffusion rate which results in limited diffusion at the electrode/electrolyte interface. This can be overcome by employing Carbyne which enhances the ion diffusion length by providing high surface area[21]. Besides the well-known form of Carbon namely diamond and graphite, the new allotropes of Carbon named Carbyne has been reported[22]. Carbyne are carbon atoms with either single and triple bond or double bond over the linear chain. These carbyne has high flexibility, superior strength and chemically stable in nature with the bandgap of about 2.56 eV[23]. Thus, these properties open up a way for supercapacitor applications. Herein, we prepared carbyne by a simple chemical route and then this was coated on nickel foam. On this carbyne coated nickel foam, FeCo<sub>2</sub>O<sub>4</sub> was grown by the solvothermal process to use as a nanohybrid electrode for supercapacitors. FeCo<sub>2</sub>O<sub>4</sub>@Carbyne is of much interest because Fe<sup>2+</sup> with variable valence state is more active than Ni<sup>2+</sup> resulting in increased specific capacitance and it has been rarely reported[24]. Carbyne when made nanohybrid with FeCo<sub>2</sub>O<sub>4</sub>, it provides enhanced electrochemical performance because of its enhanced surface area. Later, the physical and electrochemical characterizations of FeCo<sub>2</sub>O<sub>4</sub>@Carbyne nanohybrid were examined.

## **EXPERIMENTAL SECTION**

## **Chemicals Used**

Silver nitrate, ammonia and benzene were purchased from Sigma Aldrich USA. Perchloric acid, FeCl<sub>3</sub>.4H<sub>2</sub>O, Co (NO<sub>3</sub>)<sub>2</sub>.6H<sub>2</sub>O, urea and ethylene glycol were purchased from Merck, India. Distilled water was utilized throughout the reaction.

# **Preparation of Carbyne**

Initially, 0.4 g of silver nitrate was dissolved in 100ml of aqueous ammonia solution using a magnetic stirrer for 10 min. Later, 50ml of benzene was added to the above solution and then 2.5 g of calcium carbide was added until a uniform mixture was obtained. Further 3 mol/L of the perchloric acid was added to the above mixture until the nature of the solution becomes acidic. Once, the state of the solution became acidic, the reaction was kept under undisturbed conditions for 12 hours. Finally, the reaction mixture was filtered, washed and dried under vacuum at 70 °C for four hours.

# Preparation of FeCo<sub>2</sub>O<sub>4</sub>@Carbyne nanohybrid

First, the nickel foam was cleaned thoroughly to remove oxides and dirt present on it. Figure1depicts the schematic sketch of FeCo<sub>2</sub>O<sub>4</sub> @Carbyne nanohybrid. The nickel foam was immersed in 3M HCl solution for 10 min under sonication. Then, it was cleaned and dried for 30 mins. The treated nickel foam was then coated with the as-prepared carbyne and subjected to drying at 50 °C for two hours in the oven. Later, the solution containing 1mmol of FeCl<sub>3</sub>.4H<sub>2</sub>O, 2mmol of Co (NO<sub>3</sub>)<sub>2</sub>.6H<sub>2</sub>O and 50mmol of urea was prepared by dissolving them in a solution containing 30ml of ethylene glycol and 10ml of distilled water under stirring for 30min. This reaction solution was then poured into 100ml of an autoclave. To this, carbyne-coated nickel foam was immersed and maintained in a furnace at 200 °C for 24 hours to grow FeCo<sub>2</sub>O<sub>4</sub> onto carbyne coated nickel foam. This autoclave was taken out and allowed to cool naturally. Then, the carbyne coated nickel foam was separated and dried at 60 °C for 3 hours to get FeCo<sub>2</sub>O<sub>4</sub> @Carbyne nanohybrid.

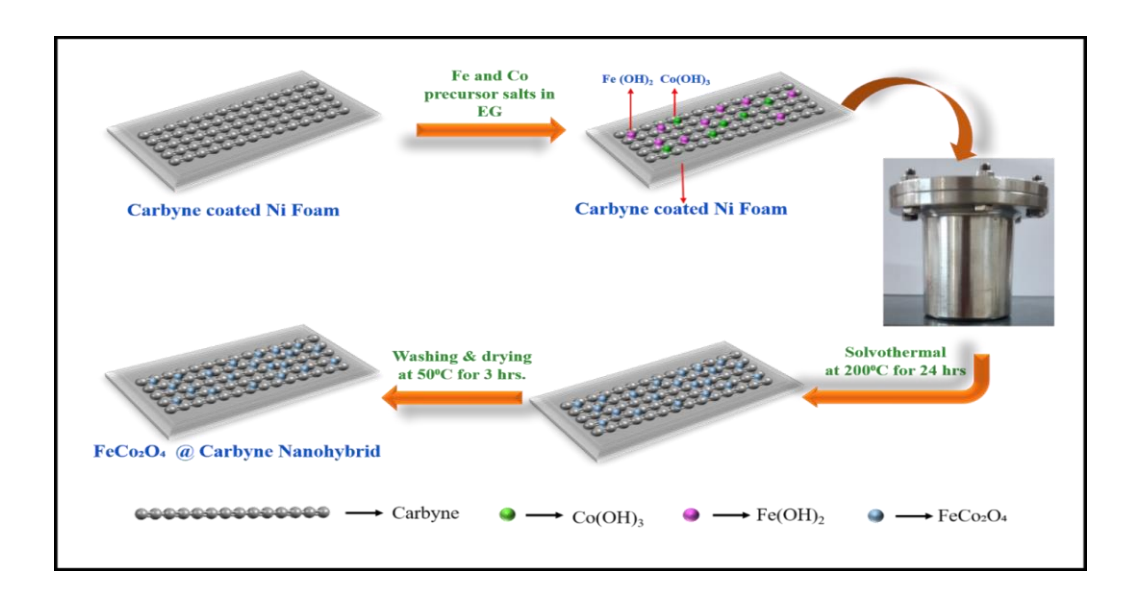


Figure 1 Schematic sketch of the synthesis of FeCo<sub>2</sub>O<sub>4</sub>@Carbyne electrode

# **Physical Characterization**

The structure and crystallinity of FeCo<sub>2</sub>O<sub>4</sub>@Carbyne nanohybrid was obtained by using an x-ray diffraction (XRD) analyzer (Rigaku, Model: Ultima IV) with a wavelength of 1.540 Å at the scan rate of 5° to 80° with an increment of 0.05°. The micro-Raman spectrometer (Renishaw RW-2000) employing Ar<sup>+</sup> laser with the wavelength of 514 nm was employed to analyze the Raman spectra. The morphology of the prepared nanostructure was investigated using field emission scanning electron microscopy studies (Carl Zeiss; Model: Sigma). In addition, the presence of elements was confirmed by energy dispersive X-ray analysis (EDAX) analysis (BRUKER). The oxidation state of the prepared nanostructure was recorded using an Ultra DLD X-ray photoelectron spectrometer (XPS) with an operating power of about 75 W.

#### **Electrochemical Characterization**

The electrochemical characterization was conducted using a three-electrode set up employing FeCo<sub>2</sub>O<sub>4</sub>@Carbyne, platinum and saturated calomel as the working, counter and reference electrode in 3M KOH electrolyte using the electrochemical analyzer (Biologic Model: VSP). The cyclic voltammetry test was performed in the potential range of -0.5 to 0.3V for scan rates ranging from 5–100 mVs<sup>-1</sup>. The galvanostatic charge-discharge test was done in the potential of -0.3 to 0.3V for a current density of 3, 5,7 and 10 Ag<sup>-1</sup>. The Electrochemical Impedance Spectroscopy (EIS) studies were carried out in the frequency range of 100 kHz to

1Hz with an amplitude of 10mV. From the GCD curve, the specific capacitance was calculated using the formula;[25]

$$C_{\rm sp} = \frac{I(\Delta t)}{m(\Delta V)} \qquad -----(1)$$

Where, I indicates current (A),  $\Delta t$  indicates discharging time (secs), m indicates the mass of electrode (g),  $\Delta V$  indicates potential difference(V).

Furthermore, the ASC device was assembled using a positive electrode made of FeCo<sub>2</sub>O<sub>4</sub>@Carbyne nanohybrid, a negative electrode made of activated carbon, and a separator made of PVDF polymer membrane soaked in 3M KOH. Later, the optimum mass ratio between both electrodes was calculated using the equation;[26]

$$\frac{m_+}{m_-} = \frac{C_{-\Delta V_-}}{C_{+\Delta V_+}} \quad ----(2)$$

Where,  $C_{+}$  and  $C_{-}$  indicate the specific capacitance (Fg<sup>-1</sup>) of both electrodes,  $\Delta V_{+}$  and  $\Delta V_{-}$  as the potential difference (V) of both electrodes, respectively. Meanwhile, the energy density and power density are obtained using the below equation;[27]

Energy Density = 
$$\frac{CV^2}{2}$$
 ----- (3)

Power Density = 
$$\frac{E_{Cell} X 3600}{\Delta t}$$
 ----- (4)

Where,  $E_{\text{cell}}$  indicates the energy density of the cell (Wh kg<sup>-1</sup>),  $\Delta t$  indicates discharge time (mins).

## RESULTS AND DISCUSSION

# Mechanism for the formation of FeCo<sub>2</sub>O<sub>4</sub> nanoparticles

During the solvothermal process, at the initial state hydrolysis of urea occurs with the liberation of ammonia and the OH<sup>-</sup> ions. These OH<sup>-</sup> ions react with metal cations to form the

mixed metal hydroxide, FeCo<sub>2</sub>(OH)<sub>6</sub>. This mixed metal hydroxide, FeCo<sub>2</sub>(OH)<sub>6</sub> upon further thermal treatment converted into FeCo<sub>2</sub>O<sub>4</sub> nanoparticles.[28]

$$H_2NCONH_2 + H_2O \rightarrow 2NH_3 + CO_2$$

$$NH_3 + H_2O \rightarrow NH_4^+ + OH^-$$

$$Fe^{2+} + 2Co^{2+} + 6OH^{-} \rightarrow FeCo_{2}(OH)_{6}$$

$$FeCo_2(OH)_6 + \frac{1}{2}O_2 \rightarrow FeCo_2O_4 + 3H_2O$$

## Mechanism for the formation of Carbyne

Initially, silver nitrate reacts with aqueous ammonia to form diamminesilver(I) nitrate which is then converted into a silver diamine complex. This diamine complex reacts with calcium carbide to form silver acetylide with the evolution of ammonia and calcium hydroxide. Later, the formed silver acetylide undergoes decomposition in presence of perchloric acid and aqueous ammonia solution to form (-C=C-) n which is further undergone polymerization to form carbyne. During this reaction, the formed ammonia and calcium hydroxide are neutralized by perchloric acid. The generated carbyne dissolved in benzene leading to the formation of carbyne with a longer chain.

$$AgNO_3 + 2NH_3.H_2O \rightarrow [Ag(NH_3)_2]NO_3 + 2H_2O$$

$$[Ag(NH_3)_2]^+ + CaC_2 + H_2O \rightarrow AgC \equiv CAg + Ca(OH)_2 + NH_3$$

$$AgC \equiv CAg + HClO_4 \xrightarrow{NH_3.H_2O} [Ag (NH_3)_2] + (-C \equiv C-) + NH_4ClO_4$$

$$n(\text{--}C \equiv C\text{---}) + Benzene \xrightarrow{Polymerization} (\text{---}C \equiv C\text{---})_n$$

From **Figure 1a** the diffraction peaks at 21.03, 31.3, 44.8, 55.8, 59.5 and 65.4 correspond to planes at (111), (220), (311), (422), (511) and (440) which are assigned to FeCo<sub>2</sub>O<sub>4</sub> with cubic structure (Fd3m space group) according to JCPDS card No: 98-009-8552 which are designated as [A(B'<sub>2</sub>)]O<sub>4</sub>[29]. In general, the formula [A(B'<sub>2</sub>)] O<sub>4</sub> indicates the binary metal oxides where A and B' corresponds to the metal cations occupying the tetrahedral or octahedral sites. In addition, **Figure 1b** depicts the XRD pattern of carbyne. The major peaks at 29.54,

34.43, 37.19, 57.08, 63.21 and 64.30 correspond to the planes at (002), (110), (111) and (113) with the hexagonal structure indicating the presence of carbyne according to the previous study[30]. All the diffraction peaks corresponding to both FeCo<sub>2</sub>O<sub>4</sub> and carbyne are present in FeCo<sub>2</sub>O<sub>4</sub>@Carbyne nanohybrid and it is shown in **Figure 1c**. Thus, the formation of FeCo<sub>2</sub>O<sub>4</sub>@Carbyne nanohybrid has been confirmed.

**Figure 1d** shows the Raman spectra of FeCo<sub>2</sub>O<sub>4</sub>, carbyne and FeCo<sub>2</sub>O<sub>4</sub>@Carbyne. In FeCo<sub>2</sub>O<sub>4</sub>@Carbyne nanohybrid, the presence of characteristic peaks at 519, 617 and 688 cm<sup>-1</sup> correspond to the E<sub>g</sub>, F<sub>2g</sub> and A<sub>1g</sub> vibrational modes of FeCo<sub>2</sub>O<sub>4</sub>. Meanwhile, the peaks at 1320 and 1569 cm<sup>-1</sup> indicate D and G bands of Carbyne, respectively[31]. Thus, the peaks corresponding to both Carbyne and FeCo<sub>2</sub>O<sub>4</sub> are present in the FeCo<sub>2</sub>O<sub>4</sub>@Carbyne nanohybrid.

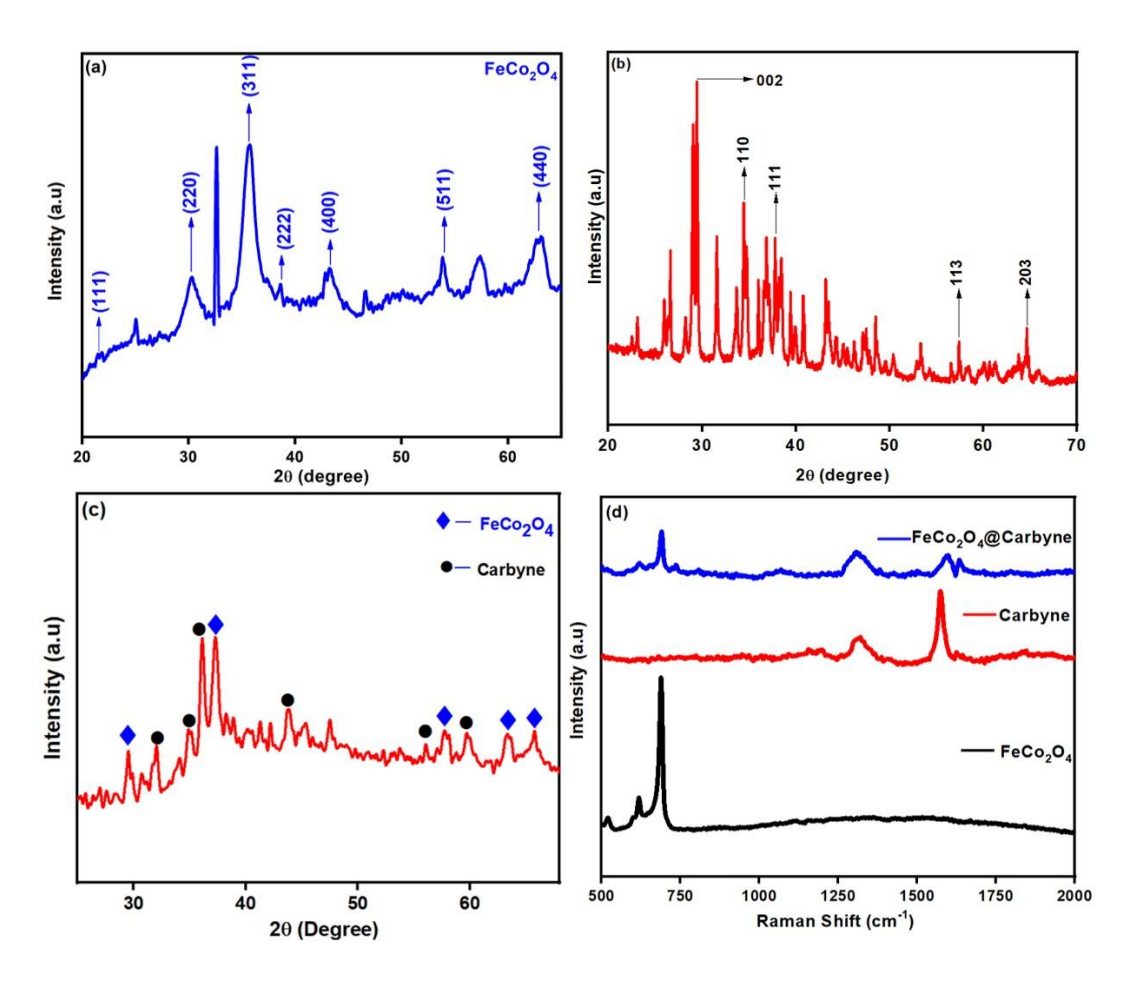


**Figure 1** XRD patternof (a) FeCo<sub>2</sub>O<sub>4</sub>, (b) Carbyne, (c) FeCo<sub>2</sub>O<sub>4</sub>@Carbyne nanohybrid, (d)Raman spectra ofFeCo<sub>2</sub>O<sub>4</sub>, Carbyne and FeCo<sub>2</sub>O<sub>4</sub>@Carbyne nanohybrid.

The morphologies of FeCo<sub>2</sub>O<sub>4</sub> and FeCo<sub>2</sub>O<sub>4</sub>@Carbyne nanohybrid were analyzed by FE-SEM analyzer. **Figure 2a** shows the morphology of as-synthesized FeCo<sub>2</sub>O<sub>4</sub> nanoparticles. Using image J software, the size of the nanoparticle is found to be  $\sim$  36nm. In addition, the morphology of FeCo<sub>2</sub>O<sub>4</sub>@Carbyne nanostructure is shown in **Figure 2b**. From **Figure 2b**, it is observed that FeCo<sub>2</sub>O<sub>4</sub> nanoparticles are decorated onto the carbyne with nanoflake structure[32]. The carbyne with nanoflake structure is grown uniformly on the nickel foamforming petal-like structure. These nanoflake morphology results in the cross-linked structure providing good mechanical strength. Thus, FeCo<sub>2</sub>O<sub>4</sub>/Carbyne nanoflakes show better electrochemical performance arising from their improved surface area, larger electroactive sites and facilitate faster ion diffusion into the electrolyte. **Figure 2c** depicts the EDAX image of FeCo<sub>2</sub>O<sub>4</sub>@Carbyne nanohybrid. The EDAX spectra indicate the prominent peaks of elements present, which confirms that the prepared FeCo<sub>2</sub>O<sub>4</sub>@Carbyne electrode consists of Fe, Co, O<sub>2</sub> and C elements. The elements present and their weight percentage are tabulated.

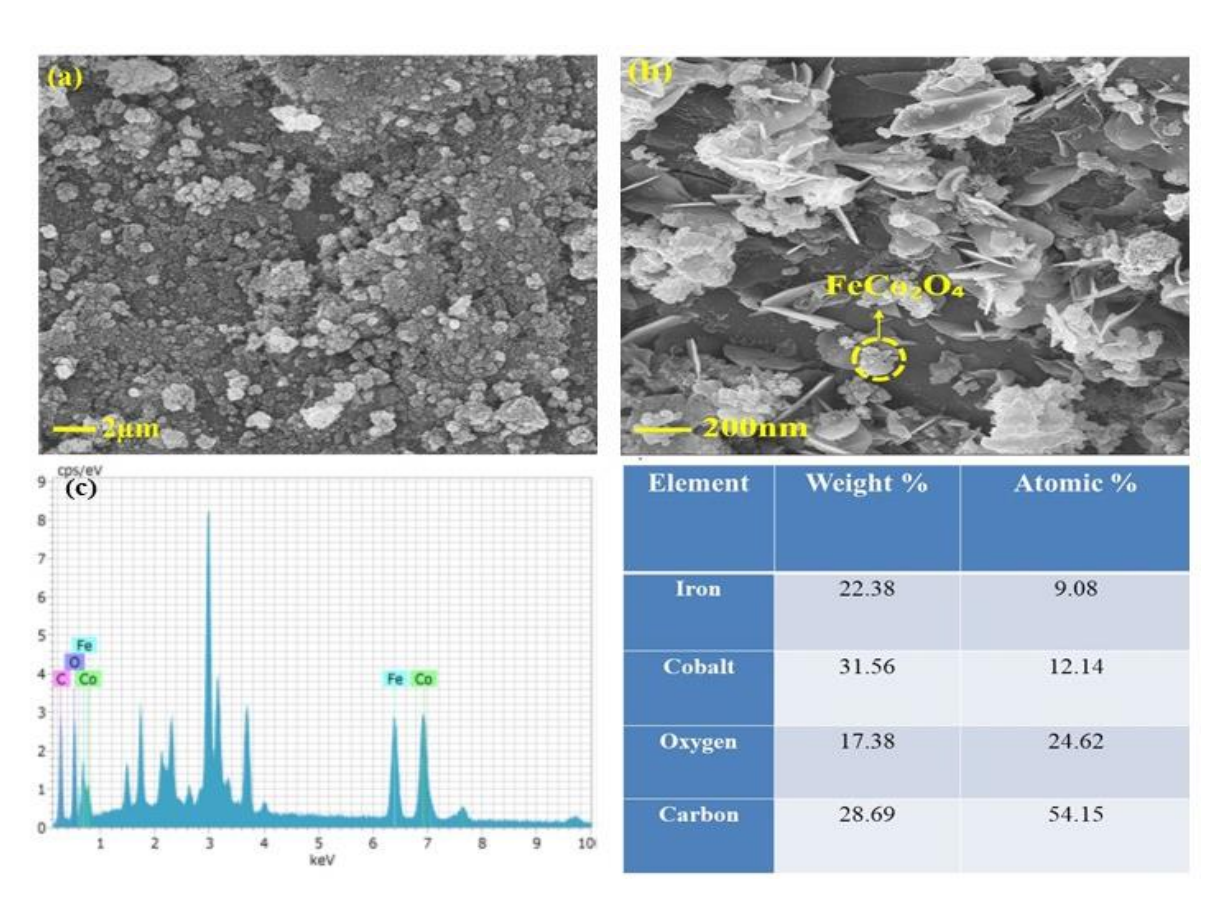


**Figure 2** FESEM image of (a) FeCo<sub>2</sub>O<sub>4</sub> and (b) FeCo<sub>2</sub>O<sub>4</sub>@Carbyne nanohybrid on Ni foam; (c) EDAX image of FeCo<sub>2</sub>O<sub>4</sub>@Carbyne nanohybrid and its elements present with weight and atomic percentages.

XPS measurements were used to analyze the surface and oxidation state of the produced FeCo<sub>2</sub>O<sub>4</sub>@carbyne nanohybrid. **Figure 3a** indicates the XPS spectra of Fe 2p with major peaks corresponding to binding energy values of 710.3eV and 723.1eV indicating Fe 2p<sub>3/2</sub> and Fe 2p<sub>1/2</sub>. In addition, the deconvoluted peaks at the binding energy values of 710.2eV and 722.8eV indicate the Fe<sup>2+</sup> while the peaks at 712.3eV and 725.4eV indicate Fe<sup>3+</sup>[29]. Thus, both Fe<sup>2+</sup> and Fe<sup>3+</sup> states coexist in FeCo<sub>2</sub>O<sub>4</sub>@carbyne. **Figure 3b** depicts the XPS spectra of Co 2p with major peaks at 779.4eV and 795.7eV indicating the presence of Co 2p<sub>3/2</sub> and Co 2p<sub>1/2</sub>. The presence of deconvoluted peaks at 781.5eV and 795.3eV corresponds to Co<sup>2+</sup>; while the peaks at 780.1eV and 795.8eV correspond to Co<sup>3+</sup>. Thus, both Co<sup>2+</sup> and Co<sup>3+</sup> states coexist in the nanohybrid electrode. **Figure 3c** displays the XPS spectra of O 1s which consists of main peaks at 529.1eV and 531.4eV. The characteristic peak at 529.1eV corresponds to the metal-oxygen bond and the other peak at 531.4eV corresponds to oxygen in OH<sup>-</sup> groups[16]. **Figure 3d** indicates the XPS spectra of C 1s which are deconvoluted into several peaks. The strongest peak centered at 284.9eV corresponds to -C≡C-C≡C- carbyne background and the peak at 291.6eV corresponds to the shake-up satellite peak which arises from the aromatic compound[33].

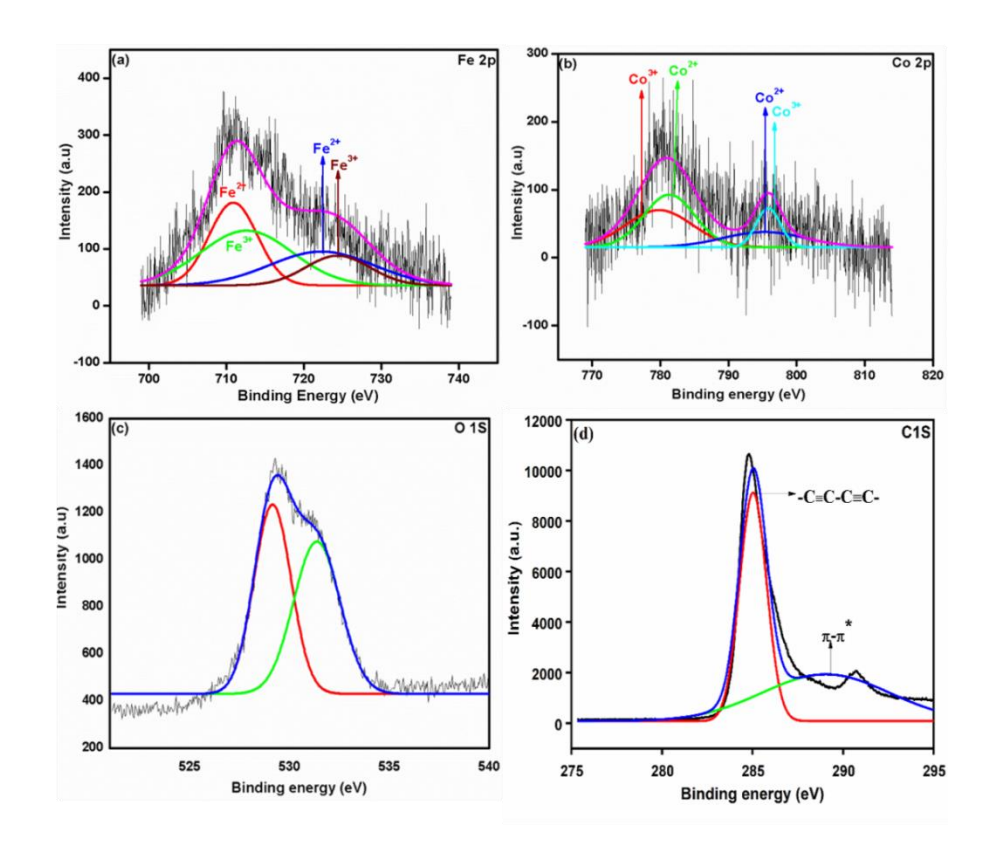


Fig.3 XPS spectrum of FeCo<sub>2</sub>O<sub>4</sub>@Carbyne (a)Fe 2p, (b) Co 2p, (c) O 1s and (d) C1s

To evaluate the electrochemical characteristics of prepared FeCo<sub>2</sub>O<sub>4</sub>@Carbyne nanohybrid, Cyclic Voltammetry, Galvanostatic Charge Discharge and Electrochemical Impedance Spectroscopy were performed. **Figure 4a** shows a typical CV curve of FeCo<sub>2</sub>O<sub>4</sub>, Carbyne and FeCo<sub>2</sub>O<sub>4</sub>@Carbyne electrodes obtained at the scan rate of 25mVs<sup>-1</sup>. From **Figure 4a** comparatively, the area enclosed by the FeCo<sub>2</sub>O<sub>4</sub>@Carbyne electrode is found to be higher than the carbyne and FeCo<sub>2</sub>O<sub>4</sub>electrode. This indicates FeCo<sub>2</sub>O<sub>4</sub>@Carbyne nanohybrid electrode maintains an increased specific capacitance than FeCo<sub>2</sub>O<sub>4</sub> and Carbyne electrodes. Besides the CV curve, it is found that carbyne undergoes EDLC behavior and FeCo<sub>2</sub>O<sub>4</sub> and FeCo<sub>2</sub>O<sub>4</sub>@Carbyne with non-rectangular shapes exhibit pseudocapacitive behavior.

**Figure 4b** elucidates the CV curve of FeCo<sub>2</sub>O<sub>4</sub>@Carbyne nanohybrid electrode obtained at different scan rates ranging from -0.5 to 0.3V. The quite different curve shape and redox peak of this electrode are not only demonstrating a pseudocapacitive nature but also reveals the addition of carbyne which plays a significant role in the electrochemical performance[22]. FeCo<sub>2</sub>O<sub>4</sub>@Carbyne nanohybrid has a typical faradaic electrochemical behavior rather than the

shape of EDLC. At a higher scan rate, the redox peak also increases revealing lower resistance of the electrode. From the CV curve, according to the power-law;

$$i = a \gamma^{b}$$
 ----(5)

where i represents redox peak (A),  $\gamma$  represents scan rate and a, b represents adjustable parameters, that are used to predict the type of the mechanism. The value of parameter b = 1 indicates the capacitive controlled process, while b = 0.5 represents diffusion-controlled process[34]. In the **inset of Figure 4b** the value of b from the redox peak was found to be 0.51, indicating that a diffusion-controlled process has occurred.

**Figure 4c** shows the galvanostatic charge-discharge curves of FeCo<sub>2</sub>O<sub>4</sub>@Carbyne nanohybrid operated between the working potential of -0.3 to 0.3V. As expected, the nanohybrid demonstrates a longer discharge time giving rise to a higher capacitance value. The specific capacitance is found to be as high as 2584.8, 2363.6, 1579.1 and 773.0 Fg<sup>-1</sup> at the current density of 3,5,7 and 10 Ag<sup>-1</sup>, respectively. Further, the presence of voltage plateaus in the GCD curve indicates the pseudocapacitive nature of the nanohybrid electrode which coincides well with the CV outputs. In addition, the symmetrical shape of the curve and the absence of iR drop reveals the excellent redox behavior with a lower internal resistance of the electrode. Table 1 shows the comparison of as-prepared FeCo<sub>2</sub>O<sub>4</sub>@Carbyne nanohybrid electrodes with FeCo<sub>2</sub>O<sub>4</sub> and their nano-composites based electrodes reported earlier in the literature <sup>14,18,19,35,37</sup>.

**Table 1**: Comparison of specific capacitance of FeCo<sub>2</sub>O<sub>4</sub>@Carbyne based electrode with earlier reported results for FeCo<sub>2</sub>O<sub>4</sub> and its nano-composites.

Electrode Material	Specific Capacitance	<b>Current Density</b>	Electrolyte	Ref.
FeCo <sub>2</sub> O <sub>4</sub> nanosheets	853.8 Fg <sup>-1</sup>	5Ag <sup>-1</sup>	1M Na <sub>2</sub> SO <sub>4</sub>	[35]
FeCo <sub>2</sub> O <sub>4</sub> nanowires	1963.0 Fg <sup>-1</sup>	2 mA cm <sup>-2</sup>	1M Na <sub>2</sub> SO <sub>4</sub>	[14]
FeCo <sub>2</sub> O <sub>4</sub> nanoflakes	433.0 Fg <sup>-1</sup>	0.1 Ag <sup>-1</sup>	2M KOH	[18]
FeCo <sub>2</sub> O <sub>4</sub> @ NiCo LDH	2426.0 Fg <sup>-1</sup>	1 Ag <sup>-1</sup>	2M KOH	[19]
FeCo <sub>2</sub> O <sub>4</sub> @ MnO <sub>2</sub>	2112.9 Fg <sup>-1</sup>	40 mA cm <sup>-2</sup>	2M KOH	[37]
FeCo <sub>2</sub> O <sub>4</sub> @Carbyne	2584.2 Fg <sup>-1</sup>	3 Ag <sup>-1</sup>	3М КОН	This work

Followed by CV and GCD, FeCo<sub>2</sub>O<sub>4</sub>@Carbyne nanohybrid electrode was subjected to EIS studies. **Figure 4d** shows EIS curves of FeCo<sub>2</sub>O<sub>4</sub>@Carbyne nanohybrid with two portions namely a semicircle followed by a vertical line. The smallest value of charge transfer resistance ( $R_{ct}$ ) obtained from the semicircle indicates that the electrode provides a larger active site and lower charge transfer resistance[38]. The presence of a straight line in the plot indicates the better capacitive behavior of the electrode with low diffusion resistance[39]. Consequently, the FeCo<sub>2</sub>O<sub>4</sub>@Carbyne nanohybrid provides charge transfer resistance ( $R_{ct}$ ) of about 0.23 $\Omega$  which is smaller than FeCo<sub>2</sub>O<sub>4</sub>of about 0. 28 $\Omega$ . Thus, the results of EIS measurements reveal the easier transportation of electrolyte ions inside the nanohybrid electrode.

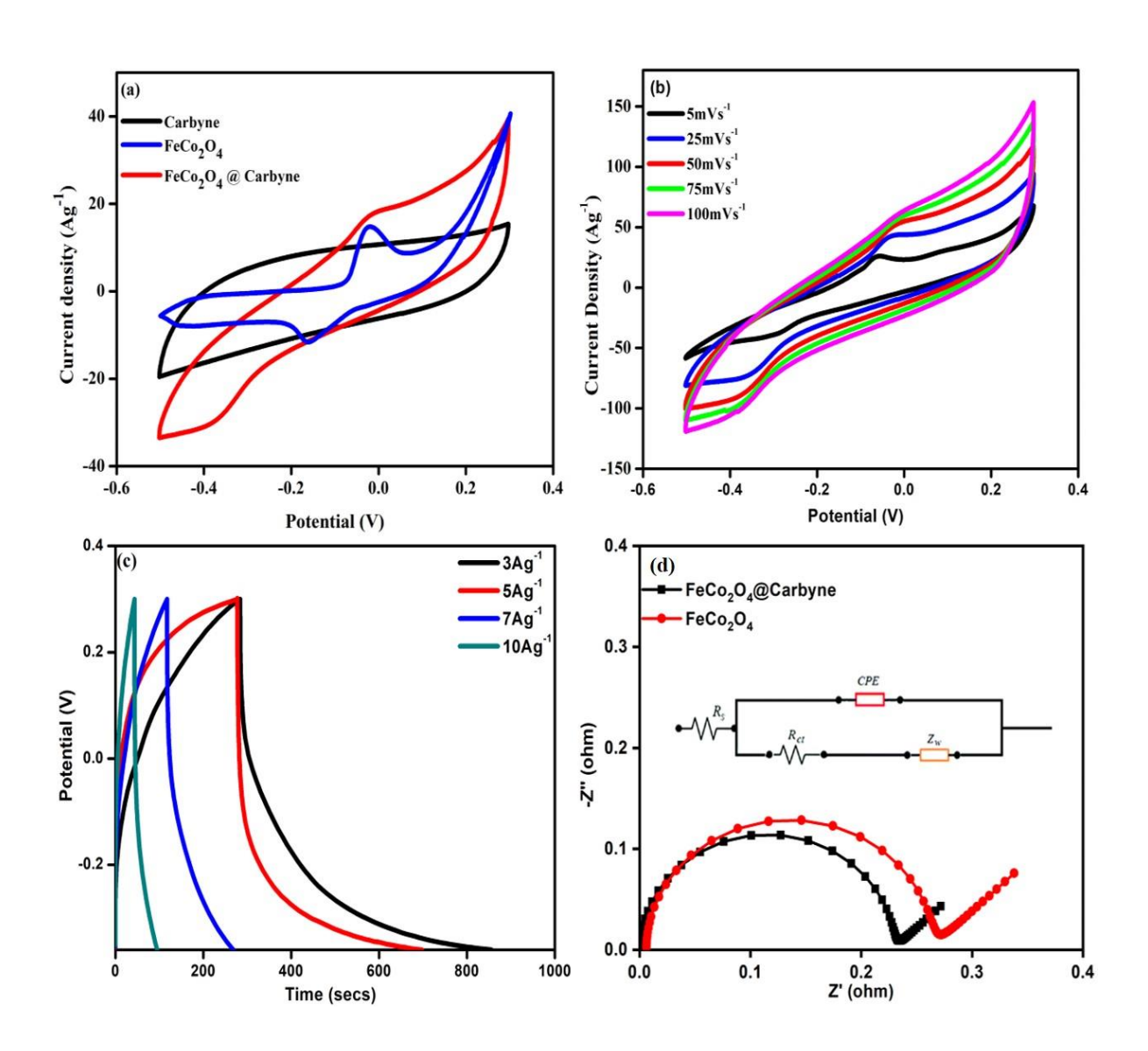


**Figure4**(a)CV curves of FeCo<sub>2</sub>O<sub>4</sub>, Carbyne and FeCo<sub>2</sub>O<sub>4</sub>@Carbyne electrode corresponding to the scan rate of 25mVs<sup>-1</sup>, (b)CV curve of FeCo<sub>2</sub>O<sub>4</sub>@Carbyne electrode at different of 5, 25, 50, 75 and 100 mVs<sup>-1</sup>, inset shows the **b**-value estimation from cathodic peak current of FeCo<sub>2</sub>O<sub>4</sub>@Carbyne electrode, (c)GCD curve of FeCo<sub>2</sub>O<sub>4</sub>@Carbyne electrode, (d)Nyquist plots of FeCo<sub>2</sub>O<sub>4</sub> and FeCo<sub>2</sub>O<sub>4</sub>@Carbyne.

As a step forward considering the superior electrochemical performance, a supercapacitor was fabricated using  $FeCo_2O_4@Carbyne$ , activated carbon (AC) as a positive and negative electrode which is designated as  $FeCo_2O_4@Carbyne$   $\parallel$  AC. To obtain the optimum mass ratio between the electrodes, the working potential of the CV studies of  $FeCo_2O_4@Carbyne$  nanohybrid and the activated carbon is studied in 3M KOH electrolyte, respectively. From the mass balance theory, [the charge accumulated on the cathode is equal to the charge accumulated on the anode], the optimal mass ratio is calculated40,41. From the equation (2), the optimal mass ratio was found to be 0.54 (m+/m-).

Figure 5a depicts the CV curve of FeCo<sub>2</sub>O<sub>4</sub>@Carbyne and AC electrodes operated in the range of -1.2 to -0.2 V and -0.5 to 0.3 V at 25 mVs-1. The typical rectangular shape of the AC represents the EDLC behavior with no obvious redox peaks in the potential range of -1.2 to -0.2 V; while the positive electrode exhibits redox peaks indicating its pseudocapacitive nature in the potential range of -0.5 to 0.3 V. Thus, the assembled asymmetric supercapacitor device is expected to be stable up to the operating potential of about 1.5 V. From the CV curve, the stable operating potential of the FeCo<sub>2</sub>O<sub>4</sub>@Carbyne | AC cell is found to be around 1.5 V. Figure 5b shows the CV curve of the FeCo<sub>2</sub>O<sub>4</sub>@Carbyne | AC obtained at scan rates of 5, 15, 25, 50, 75 and 100 mVs-1 in the range of 0 to 1.5 V. The non-rectangular shape of the CV curve indicates that the device undergoes both EDLC and pseudocapacitive behavior. In addition, at a higher scan rate, the area occupied by the curve seems to be increased and the uniformity of the CV curve was well maintained. The uniformity of the CV curve indicates the excellent capacitive behavior and reversibility of the electrodes. Figure 5c represents the GCD curve of the FeCo<sub>2</sub>O<sub>4</sub>@Carbyne | AC device obtained at different current densities. From the GCD curve, the specific capacitance was found to be 309.11, 277.36, 252.12 and 230.41 Fg<sup>-1</sup> at 3, 5, 7 and 10 Ag-1 respectively. The presence of voltage plateaus indicates that the device undergoes a Faradaic reaction which coincides well with CV curves. In addition, the curves are almost

symmetric indicating good reversible electrochemistry of the fabricated device. Further, cycling stability is the key parameter that must be accounted for the fabricated device. **Figure 5d** represents the cyclic stability of the device conducted at the current density of 10 Ag<sup>-1</sup> over 5000 cycles. The specific capacitance of the device is well maintained during the initial cycles, which shows a decrease in the later cycles exhibiting capacitance retention of 85.48% over 5000 cycles. Even after a long life of 5000 cycles, the fabricated device maintained good reversibility with Coulombic efficiency of above 100% with undistorted and symmetric curves. Thus, the excellent capacitive behavior is due to the synergistic effect of both carbyne and FeCo2O4 nanostructures.

To quantitatively analyze the interfacial performance at the electrode-electrolyte interface, an EIS test was conducted. Figure 5e elucidates the Nyquist plots of the device before and after 5000 cycles in the frequency range of 100 kHz to 1 Hz at an amplitude of 10 mV. The values of bulk solution resistance (Rs) before and after 5000 cycles are found to be 1.06 and 1.34, respectively. The value of R<sub>s</sub> is obtained by real axis intercepts which arise due to, contact resistance of the electrode, electrolyte resistance and inherent resistance. Besides, to carry out a relation between energy and power density of the fabricated device, the Ragone plot is obtained. Figure 5f elucidates the Ragone plot of the fabricated device. The energy density of the fabricated device is found to be 96.59 Whkg-1 at the power density of 2.25 kWkg-1. Subsequently, even at the high current density of 10 Ag<sup>-1</sup>, the energy density is well maintained up to 72 Whkg<sup>-1</sup> at the power density of about 7.50 kWkg<sup>-1</sup>. The above outcomes reveal that the fabricated device suits for moderate energy density application due to its stability at both low and high current densities. The energy and power densities exhibited by FeCo<sub>2</sub>O<sub>4</sub>@Carbyne || AC device shows superior performance than other reported FeCo<sub>2</sub>O<sub>4</sub> and their composites such as FeCo<sub>2</sub>O<sub>4</sub>@MnO<sub>2</sub> || AC [22 Wh kg<sup>-1</sup>/0.40kW kg<sup>-1</sup>], MnO<sub>2</sub> || rGO/FeCo<sub>2</sub>O<sub>4</sub> [46 Wh kg<sup>-1</sup>/3.60kW  $kg^{\text{-}1}]$  and  $FeCo_2O_4\, ||\, FeCo_2O_4\, [94 \ Whkg^{\text{-}1}/0.13kW \ kg^{\text{-}1}].$ 

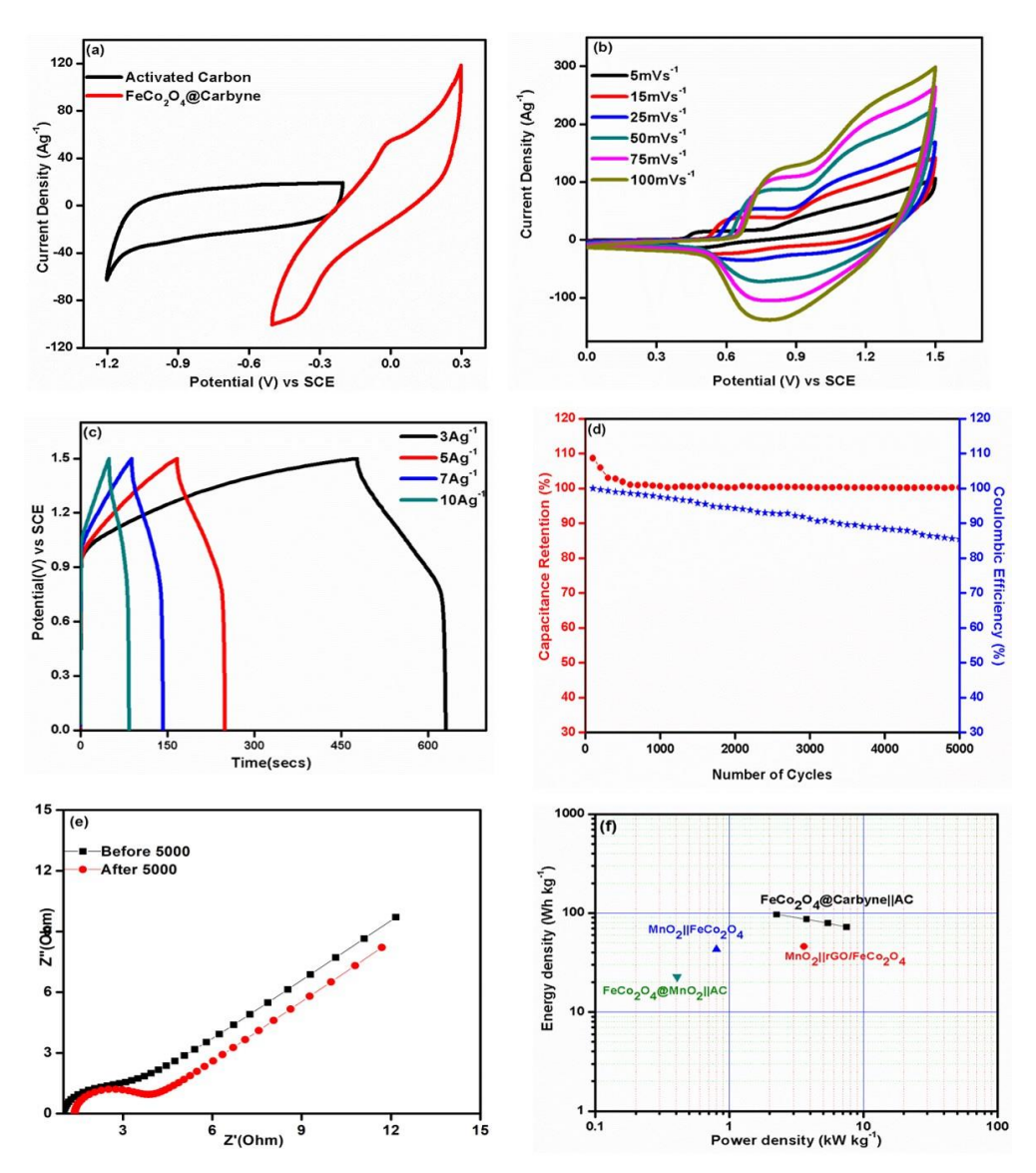


**Figure 5** (a) CV curves of FeCo<sub>2</sub>O<sub>4</sub>@Carbyne and activated carbon electrode at the scan rate of 50mVs<sup>-1</sup>, (b) CV curves of the supercapacitor device obtained at various scan rates, (c) GCD curves of the supercapacitor device obtained at various current densities, (d) Cyclic stability of supercapacitor device, (e)Nyquist plots of supercapacitor device before and after 5000 cycles, (f) Ragone plots

## **CONCLUSION**

In summary, FeCo<sub>2</sub>O<sub>4</sub>@Carbyne nanohybrid is synthesized by a two-step method to serve as an efficient electrode for supercapacitors. The crystallinity of the FeCo<sub>2</sub>O<sub>4</sub>@Carbyne nanohybrid electrode was confirmed by XRD analysis. The morphology of FeCo<sub>2</sub>O<sub>4</sub>@Carbyne

is investigated by FE-SEM analysis. Due to the combined effect of both Carbyne and FeCo<sub>2</sub>O<sub>4</sub>, the FeCo<sub>2</sub>O<sub>4</sub>@Carbyne nanohybrid results in a specific capacitance of about 2584.77 Fg<sup>-1</sup> in 3M KOH electrolyte with superior electrochemical performance. Further, the fabricated device namely FeCo<sub>2</sub>O<sub>4</sub>@Carbyne||AC exhibits a higher specific capacitance of 309.1 Fg<sup>-1</sup>with excellent cyclic stability. In addition, it offers an energy density of 96.59 Wh kg<sup>-1</sup> corresponding to the power density of 2.25 kWkg<sup>-1</sup>. Thus, the increased capacitive characteristics of FeCo<sub>2</sub>O<sub>4</sub>@Carbyne overlaid a way for their usage in supercapacitor applications.

## **CONFLICT OF INTEREST**

The authors declare no conflict of interest.

#### **ACKNOWLEDGMENTS**

AS gratefully acknowledges the UGC, New Delhi for their financial support under the BSR Mid-Career Award Scheme (No. F.19- 214/2018). TD acknowledges the United States National Science Foundation for the funding through EiR (DMR-2100946) and PREM (DMR-2122147) Awards.

## **REFERENCES**

- [1] M. Pathak, J.R. Jose, B. Chakraborty, C.S. Rout, High performance supercapacitor electrodes based on spinel NiCo2O4@MWCNT composite with insights from density functional theory simulations, J. Chem. Phys. 152 (2020). https://doi.org/10.1063/1.5138727.
- [2] N.R. Chodankar, H.D. Pham, A.K. Nanjundan, J.F.S. Fernando, K. Jayaramulu, D. Golberg, Y.K. Han, D.P. Dubal, True Meaning of Pseudocapacitors and Their Performance Metrics: Asymmetric versus Hybrid Supercapacitors, Small. 16 (2020) 1–35. https://doi.org/10.1002/smll.202002806.
- [3] D.P. Dubal, N.R. Chodankar, D.H. Kim, P. Gomez-Romero, Towards flexible solid-state supercapacitors for smart and wearable electronics, Chem. Soc. Rev. 47 (2018) 2065–2129. https://doi.org/10.1039/c7cs00505a.
- [4] X. Lu, M. Yu, G. Wang, Y. Tong, Y. Li, Flexible solid-state supercapacitors: Design,

- fabrication and applications, Energy Environ. Sci. 7 (2014) 2160–2181. https://doi.org/10.1039/c4ee00960f.
- [5] X. Wang, X. Lu, B. Liu, D. Chen, Y. Tong, G. Shen, Flexible energy-storage devices: Design consideration and recent progress, Adv. Mater. 26 (2014) 4763–4782. https://doi.org/10.1002/adma.201400910.
- [6] M. Winter, R.J. Brodd, What are batteries, fuel cells, and supercapacitors?, Chem. Rev. 104 (2004) 4245–4269. https://doi.org/10.1021/cr020730k.
- [7] P. Simon, Y. Gogotsi, B. Dunn, Where do batteries end and supercapacitors begin?, Science (80-.). 343 (2014) 1210–1211. https://doi.org/10.1126/science.1249625.
- [8] A. González, E. Goikolea, J.A. Barrena, R. Mysyk, Review on supercapacitors: Technologies and materials, Renew. Sustain. Energy Rev. 58 (2016) 1189–1206. https://doi.org/10.1016/j.rser.2015.12.249.
- [9] C. Liu, F. Li, M. Lai-Peng, H.M. Cheng, Advanced materials for energy storage, Adv. Mater. 22 (2010) 23–26. https://doi.org/10.1002/adma.200903328.
- [10] L. Zhang, X.S. Zhao, Carbon-based materials as supercapacitor electrodes, Chem. Soc. Rev. 38 (2009) 2520–2531. https://doi.org/10.1039/b813846j.
- [11] W. Gu, G. Yushin, Review of nanostructured carbon materials for electrochemical capacitor applications: Advantages and limitations of activated carbon, carbide-derived carbon, zeolite-templated carbon, carbon aerogels, carbon nanotubes, onion-like carbon, and graphene, Wiley Interdiscip. Rev. Energy Environ. 3 (2014) 424–473. https://doi.org/10.1002/wene.102.
- [12] V. Augustyn, P. Simon, B. Dunn, Pseudocapacitive oxide materials for high-rate electrochemical energy storage, Energy Environ. Sci. 7 (2014) 1597–1614. https://doi.org/10.1039/c3ee44164d.
- [13] N.R. Chodankar, D.P. Dubal, S.H. Ji, D.H. Kim, Highly efficient and stable negative electrode for asymmetric supercapacitors based on graphene/FeCo2O4 nanocomposite hybrid material, Electrochim. Acta. 295 (2019) 195–203. https://doi.org/10.1016/j.electacta.2018.10.125.
- [14] N.R. Chodankar, D.P. Dubal, Y. Kwon, D.H. Kim, Direct growth of feco2o4 nanowire arrays on flexible stainless steel mesh for high-performance asymmetric supercapacitor, NPG Asia Mater. 9 (2017) 1–10. https://doi.org/10.1038/am.2017.145.

- [15] C. Yuan, H. Bin Wu, Y. Xie, X.W. Lou, Mixed transition-metal oxides: Design, synthesis, and energy-related applications, Angew. Chemie Int. Ed. 53 (2014) 1488–1504. https://doi.org/10.1002/anie.201303971.
- [16] F. Zhu, Y. Liu, M. Yan, W. Shi, Construction of hierarchical FeCo2O4@MnO2 core-shell nanostructures on carbon fibers for high-performance asymmetric supercapacitor, J. Colloid Interface Sci. 512 (2018) 419–427. https://doi.org/10.1016/j.jcis.2017.09.093.
- [17] Z. Wang, P. Hong, S. Peng, T. Zou, Y. Yang, X. Xing, Z. Wang, R. Zhao, Z. Yan, Y. Wang, Co(OH) 2 @FeCo 2 O 4 as electrode material for high performance faradaic supercapacitor application, Electrochim. Acta. 299 (2019) 312–319. https://doi.org/10.1016/j.electacta.2019.01.017.
- [18] S.G. Mohamed, C.J. Chen, C.K. Chen, S.F. Hu, R.S. Liu, High-performance lithium-ion battery and symmetric supercapacitors based on FeCo2O4 nanoflakes electrodes, ACS Appl. Mater. Interfaces. 6 (2014) 22701–22708. https://doi.org/10.1021/am5068244.
- [19] X. He, R. Li, J. Liu, Q. Liu, R.R. chen, D. Song, J. Wang, Hierarchical FeCo2O4@NiCo layered double hydroxide core/shell nanowires for high performance flexible all-solid-state asymmetric supercapacitors, Chem. Eng. J. 334 (2018) 1573–1583. https://doi.org/10.1016/j.cej.2017.11.089.
- [20] X. Liu, F. Wei, Y. Sui, J. Qi, Y. He, Q. Meng, Polyhedral ternary oxide FeCo2O4: A new electrode material for supercapacitors, J. Alloys Compd. 735 (2018) 1339–1343. https://doi.org/10.1016/j.jallcom.2017.11.251.
- [21] X. He, Y. Zhao, R. Chen, H. Zhang, J. Liu, Q. Liu, D. Song, R. Li, J. Wang, Hierarchical FeCo2O4@polypyrrole Core/Shell Nanowires on Carbon Cloth for High-Performance Flexible All-Solid-State Asymmetric Supercapacitors, ACS Sustain. Chem. Eng. 6 (2018) 14945–14954. https://doi.org/10.1021/acssuschemeng.8b03440.
- [22] B. Pan, J. Xiao, J. Li, P. Liu, C. Wang, G. Yang, Materials: Carbyne with finite length: The one-dimensional sp carbon, Sci. Adv. 1 (2015) 1–11. https://doi.org/10.1126/sciadv.1500857.
- [23] T.C. Dinadayalane, L. Gorb, H. Dodziuk, J. Leszczynski, Modelling of the stabilization of the complex of a single walled (5,5) carbon nanotube C60H20 with cumulenic or acetylenic chain, AIP Conf. Proc. 786 (2005) 436–439. https://doi.org/10.1063/1.2103904.
- [24] B. Zhu, S. Tang, S. Vongehr, H. Xie, X. Meng, Hierarchically MnO2-Nanosheet Covered

- Submicrometer-FeCo2O4-Tube Forest as Binder-Free Electrodes for High Energy Density All-Solid-State Supercapacitors, ACS Appl. Mater. Interfaces. 8 (2016) 4762–4770. https://doi.org/10.1021/acsami.5b11367.
- [25] A.A. Mirghni, M.J. Madito, K.O. Oyedotun, T.M. Masikhwa, N.M. Ndiaye, S.J. Ray, N. Manyala, A high energy density asymmetric supercapacitor utilizing a nickel phosphate/graphene foam composite as the cathode and carbonized iron cations adsorbed onto polyaniline as the anode, RSC Adv. 8 (2018) 11608–11621. https://doi.org/10.1039/c7ra12028a.
- [26] S. Arunachalam, B. Kirubasankar, V. Murugadoss, D. Vellasamy, S. Angaiah, Facile synthesis of electrostatically anchored Nd(OH)3 nanorods onto graphene nanosheets as a high capacitance electrode material for supercapacitors, New J. Chem. 42 (2018) 2923–2932. https://doi.org/10.1039/c7nj04335j.
- [27] B. Kirubasankar, P. Palanisamy, S. Arunachalam, V. Murugadoss, S. Angaiah, 2D MoSe2-Ni(OH)2 nanohybrid as an efficient electrode material with high rate capability for asymmetric supercapacitor applications, Chem. Eng. J. 355 (2019) 881–890. https://doi.org/10.1016/j.cej.2018.08.185.
- [28] N.R. Chodankar, D.P. Dubal, Y. Kwon, D.-H. Kim, Direct growth of FeCo2O4 nanowire arrays on flexible stainless steel mesh for high-performance asymmetric supercapacitor, NPG Asia Mater. 9 (2017) e419–e419. https://doi.org/10.1038/am.2017.145.
- [29] S.G. Mohamed, S.Y. Attia, H.H. Hassan, Spinel-structured FeCo2O4 mesoporous nanosheets as efficient electrode for supercapacitor applications, Microporous Mesoporous Mater. 251 (2017) 26–33. https://doi.org/10.1016/j.micromeso.2017.05.035.
- [30] F. Cataldo, A study on the structure and electrical properties of the fourth carbon allotrope: Carbyne, Polym. Int. 44 (1997) 191–200. https://doi.org/10.1002/(SICI)1097-0126(199710)44:2<191::AID-PI842>3.0.CO;2-Y.
- [31] V.A. Online, B. Duan, W. Wang, A. Wang, K. Yuan, Z. Yu, H. Zhao, J. Qiu, Y. Yang, lithium / sulfur batteries, (2013) 13261–13267. https://doi.org/10.1039/c3ta12634j.
- [32] V.M. Melnitchenko, B.N. Smirnov, V.P. Varlakov, Y.N. Nikulin, A.M. Sladkov, Lamellar morphology and inner structure of crystalline carbyne fragemnts, Carbon N. Y. 21 (1983) 131–133. https://doi.org/10.1016/0008-6223(83)90168-9.
- [33] G. Galeotti, M. Ebrahimi, J. Lipton-Duffin, J.M. Macleod, S. Rondeau-Gagné, J.F. Morin,

- F. Rosei, 2D Supramolecular networks of dibenzonitrilediacetylene on Ag(111) stabilized by intermolecular hydrogen bonding, Phys. Chem. Chem. Phys. 19 (2017) 10602–10610. https://doi.org/10.1039/c7cp01058c.
- [34] K.V. Sankar, R.K. Selvan, D. Meyrick, Electrochemical performances of CoFe2O4 nanoparticles and a rGO based asymmetric supercapacitor, RSC Adv. 5 (2015) 99959–99967. https://doi.org/10.1039/c5ra14938j.
- [35] S.G. Mohamed, S.Y. Attia, H.H. Hassan, Spinel-structured FeCo2O4 mesoporous nanosheets as efficient electrode for supercapacitor applications, Microporous Mesoporous Mater. 251 (2017) 26–33. https://doi.org/10.1016/j.micromeso.2017.05.035.
- [36] M. Serhan, M. Sprowls, D. Jackemeyer, M. Long, I.D. Perez, W. Maret, N. Tao, E. Forzani, Total iron measurement in human serum with a smartphone, AIChE Annu. Meet. Conf. Proc. 2019-Novem (2019). https://doi.org/10.1039/x0xx00000x.
- [37] L. Lin, S. Tang, S. Zhao, X. Peng, N. Hu, Hierarchical three-dimensional FeCo2O4@MnO2 core-shell nanosheet arrays on nickel foam for high-performance supercapacitor, Electrochim. Acta. 228 (2017) 175–182. https://doi.org/10.1016/j.electacta.2017.01.022.
- [38] Q. Wang, X. Wang, J. Xu, X. Ouyang, X. Hou, D. Chen, R. Wang, G. Shen, Flexible coaxial-type fiber supercapacitor based on NiCo2O4 nanosheets electrodes, Nano Energy. 8 (2014) 44–51. https://doi.org/10.1016/j.nanoen.2014.05.014.
- [39] L. Abbasi, M. Arvand, Engineering hierarchical ultrathin CuCo 2 O 4 nanosheets array on Ni foam by rapid electrodeposition method toward high-performance binder-free supercapacitors, Appl. Surf. Sci. 445 (2018) 272–280. https://doi.org/10.1016/j.apsusc.2018.03.193.

Conflict of Interest

No competing financial interest.